AIAA JOURNAL
Vol. 39, No. 9, September 2001

Elastic-Dynamic Rotor Blade Design with Multiobjective Optimization

Jong-Eun Kim* and Nesrin Sarigul-Klijn†
University of California, Davis, Davis, California 95616

An efficient multidisciplinary design optimization methodology is applied in the design of a rotor blade to meet minimum weight, minimum vibration, and maximum material strength requirements. The design study is a high-aspect-ratio articulated flexible blade with a thin-walled multicell cross section at high tip Mach numbers. The rotor blade analysis consists of two subsets to increase efficiency in numerical methods used in each discipline. The first subset is an elastic analysis using an idealized model by chordwise segments and spanwise elements, which can provide efficient material reassignment for minimum weight design. The second subset is a dynamic analysis for optimal natural frequency placement and vibratory vertical hub shear reduction. A high-order finite element from the gradient adaptive transfinite element family formulated by the second author is used to reduce computational requirements and to improve results without increasing the number of elements. The optimization procedure is decomposed into two levels for efficient handling of the design variables and objective functions and their correlation. In level 1, the goal is the design for the minimum weight and maximum material strength simultaneously using the multiobjective optimization technique. In level 2, the goal is the design for the minimum vibratory vertical hub shear load using the modal shaping technique. The numerical results show the efficiency of the analytical methods, the usefulness of the multilevel and multiobjective function optimization, and the effects of tuning masses and their locations on the hub shear reduction.

Nomenclature

A_{cross}	=	cross-sectional area of airfoil
A_i	=	area of ith longitudinal
A_i^{SC}	=	area enclosed by two adjacent longitudinals and origin
A_i^0	=	modulus-weighted area of ith longitudinal
A_{root}	=	cross-sectional area of blade root
a	=	lift curve slope
c	=	blade chord
$c_{m,\text{AC}}$	=	moment coefficient at aerodynamic center (AC)
D_i	=	density of ith longitudinal
e	=	hinge offset
h_j^0	=	modulus-weighted thickness of jth web
I_{yy}^{MC}, I_{zz}^{MC}	=	moment of inertia about moment center(MC)
n	=	number of blades
q_{TI}	=	shear flows on each cell due to torque
$(q_z)_j$, $(q_y)_j$	=	shear flows on ith web due to shear force
R	=	blade radius
R_r	=	root radius
t_i	=	thicknesses of each segment
t_r	=	root wall thickness of ellipsoid cross section
W_k	=	weight of each spanwise element
x	=	spanwise direction
Y_{cg}, Z_{cg}	=	center of gravity coordinates
Y_i, Z_i	=	distance of ith longitudinal from reference frame y and z
Y_{MC}, Z_{MC}	=	MC coordinates
Y_{SC}, Z_{SC}	=	shear center (SC) coordinates
y	=	chordwise direction
z	=	normal direction to x–y plane
Θ	=	blade collective pitch angle
ρ_∞	=	air density
σ	=	rotor solidity, $nc/\pi R$
Ω	=	rotor angular velocity

Subscripts

i	=	longitudinal index
j	=	idealized web index
k	=	spanwise element index
l	=	cell index

Introduction

MULTIDISCIPLINARY design optimization has been used in complex design problems such as rotating blade design, which involves elasticity, aerodynamics, and structural dynamics and their strong interaction. The changes of mass and stiffness distribution along blade chord and span direction affect the structural dynamics and aeroelastic behavior as well as the stress distribution. One of the goals in a rotorcraft blade design is to reduce the weight while minimizing vibrations transmitted to the hub. Furthermore, the blade must have sufficient strength, stiffness, and inertia to satisfy all of the mission requirements.

The research history on the application of optimization tools to rotor blade design is well summarized in Refs. 1–4. Peters et al.[5,6] introduced a minimum weight design together with autorotational inertia to ensure sufficient inertia and proper blade natural frequencies to separate them from the aerodynamic forcing frequencies through optimal blade mass and stiffness distributions. The optimization procedure was divided into two steps. In the first step, the frequency placement was taken as an objective function with appropriate structural constraints to minimize the discrepancies between desired and actual frequencies. In second step, the blade weight was minimized with frequency windows as constraints. The thicknesses and dimensions of the box beam, which represented blade cross section, together with lumped mass and tip weight were considered as the design variables. The program CONMIN[7] was used as an optimizer.

Friedmann[8] presented the structural optimization for vibration reduction using a box beam model with tuning weights and lumped masses. The design variables were the breadth, height, and their thicknesses of a thin-walled rectangular box beam. The natural frequency placement and aeroelastic stability were included in the constraints, and the maximum value of oscillatory hub vertical shear and moment were the objective functions. A sequence of unconstrained minimization technique based on an extended interior penalty function was used for the optimization.

Received 27 December 1999; revision received 1 July 2001; accepted for publication 31 July 2001.

*Graduate Research Assistant, Department of Mechanical and Aeronautical Engineering. Student Member AIAA.

†Professor, Department of Mechanical and Aeronautical Engineering. Associate Fellow AIAA.

Walsh et al.[9] tried an optimal aerodynamic design to minimize the hover horsepower by satisfying the hover and forward flight performance through exploring the influence of rotor blade design parameters such as twist, blade radius, tip speed, chord distribution, taper ratio, sweep, and airfoil section. Chattopadhyay and Walsh[10] investigated minimum weight design, using rather simplified box beam model. The rectangular and tapered box beam dimension, horizontal and vertical wall thicknesses, and nonstructural lumped masses on 10 spanwise segments were taken as the design variables. The constraints were placed on the blade autorotational inertia and the natural frequencies of the blade. Their extended study[11] conducted a multiobjective function optimization for minimum weight and minimum vertical hub shear load simultaneously. Centrifugal stress was considered as an additional constraint. The design variables were the bending and torsion stiffnesses of the blade cross section and taper ratio.

Weller and Davis[12] compared their numerical optimization results with wind-tunnel tests for the purpose of improving vibratory characteristics. Analytical optimization procedures were used to minimize hub modal shears and modal vibration indices with mass and stiffness distributions as the design variables. They found that frequency placement criteria alone were inadequate to achieve minimum vibratory rotor designs. Celi and Friedmann[13] compared the results of straight and swept blade tips using structural optimization to minimize vertical hub shears in forward flight with single- and double-cell cross section models. Aeroelastic stability and autorotational inertia were imposed as constraints. The use of tip sweep as an additional design variable allowed a further reduction of the objective function compared to a straight tip.

Lim and Chopra[14] addressed the aeroelastic optimization of hingeless rotors using CONMIN along with an efficient sensitivity analysis. The design variables were the dimensions of the box beam, chordwise location of blade center of gravity, nonstructural mass, and blade bending stiffness. A finite element method in space and time was used for the aeroelastic analysis of rotors. The objective functions were defined as the components of oscillatory hub loads and aeroelastic stability. Adelman and Mantay[15] described integrated multidisciplinary rotorcraft design optimization of NASA/Army research activity using a simple box beam cross section model and showed the interactions among disciplines. He and Peters[16] attempted an integrated analysis of structural, dynamics, and aerodynamics for optimum rotor blade design. They investigated optimum dynamic and aerodynamic performance by natural frequency placement and by proper blade planform and spanwise twist, respectively. The failure and fatigue stresses were also included in the constraints. Ganguli and Chopra[17] performed aeroelastic and sensitivity analyses using either one-cell or two-cell composite box beam models to minimize the hub load with constraints on frequency placement and aeroelastic stability. Yuan and Friedmann[18] also investigated the effects swept tips on vibratory hub loads using the composite blades. The aeroelastic analysis was based on a moderate deflection finite element model.

The rotorcraft blade can be modeled as an elastic beam attached to a rigid hub. A high aspect ratio flexible blade with a thin-walled cross section undergoes elastic deformation in axial, bending, and torsion under high rotational speed. An efficient analytical tool for the accurate stress prediction is required to impose material strength criteria on the optimization procedure as a constraint or an objective function. Until the present work, a typical equivalent box beam model has been widely used by researchers to represent blade cross section, and the stiffness and mass of the leading and trailing edges were included partially or neglected in the analysis.

The purpose of this research is to present an integrated rotor blade design method to achieve the minimum weight, minimum vibration, and maximum material strength objectives by using an efficient multilevel and multiobjective function optimization technique. The design study is a high aspect ratio articulated flexible blade with a thin-walled multicell cross section at high tip Mach numbers. In this research, the rotor blade analysis sets consist of two subsets, which will increase efficiency in numerical methods used in each discipline. The design variables, objective functions, and constraints used in the optimization process are from these two subsets.

The first subset is an elastic analysis using an idealized model. To minimize the geometry errors in chord direction, all portions of the blade cross section are divided into a number of segments so that their mass and stiffness can be taken into account in the analysis. Then the segments are idealized as effective webs and areas of longitudinals. This idealized model allows systematic calculations of not only the cross-sectional properties but also the chordwise locations of the shear center, moment center, and center of gravity precisely. These centers are considered as constraints to be placed at optimal locations. To evaluate all stress components and their distributions, the blade is also divided into many numbers of elements along the span direction. A new stress prediction method is introduced. This method begins with an assumption of spanwise deflection precisely using a second-order polynomial and then the calculation of the unknown coefficients of polynomial and coning angle at the hinge from the boundary and a static stability conditions. This approach allows the evaluations of the axial stresses due to high centrifugal force and bending moment and shear stresses due to shear force and twisting moment. The combined blade element and momentum theories are used for calculation of aerodynamic force and moment.[19]

The second subset is a dynamic analysis using the finite element method. The dynamic analysis is required to separate the blade natural frequencies from the multiples of forcing frequency to minimize the transmission of harmonic oscillation to the hub. Taylor[20] developed a strategy of vibration hub shear reduction through the modal shaping technique. Pritchard and Adelman[21] investigated optimal tuning masses and their locations for hub shear reduction based on finite element formulation. This methodology is applied here to verify the effects of tuning masses and their locations on hub shear reduction. A high-order finite element from the gradient adaptive transfinite element (GATE) family is used to obtain more accurate results with less computational requirements.[22,23] The equivalent plate thicknesses, which have the same area and moment of inertia as the arbitrary airfoil, can be separate input data for each mass and stiffness matrix of the plate finite element for the purpose of remarkably reducing the computational cost for the dynamic analysis.

A multilevel and multiobjective optimization is applied for efficient handling of the design variables and the objective functions together with their correlation. In level 1, primary design is conducted using the thicknesses of the segments and root wall thickness together with thickness variation ratio as the design variables. The goal is the design for the minimum weight and maximum material margin of safety simultaneously using the multiobjective function optimization technique.[11,24] In level 2, secondary design is conducted using the tuning masses and their locations as a new design variable set. The goal is the design for the minimum vibratory vertical hub shear. The final values of the design variables of level 1 optimization are initial values for level 2 optimization as the fixed parameters. The results of this approach are compared with other multiobjective function optimization techniques such as utility function formulation and global criterion formulation.[24] The autorotational inertia, maximum twisting angle, and blade tip deflection are also included in the constraints. The program CONMIN[7] is used as optimizer. This newly introduced approach is demonstrated to be geometrically correct as well as being computationally efficient.

Governing Equations for Elastic Analysis

Idealized Rotor Blade Cross Section

The articulated rotorcraft blade can be modeled as an elastic beam attached to a rigid hub with a flapwise hinge. Figure 1 shows four-blade rotor system with rectangular planform, and section B–B shows the cross section profile of the connector designed as an ellipsoid shape in this research. The connector, called blade root, should have enough strength to endure high centrifugal force. When a low-aspect-ratio blade rotates with a low speed, the blade can be considered as a rigid body neglecting the elastic deformations and the stress component due to bending moment. In a design, however, where a high-aspect-ratio blade rotates with high tip speed, an analytical tool for accurate stress prediction that includes the elastic deformations and all stress components is required to achieve minimum weight.

A box beam model using width w, height h, and their thicknesses shown in Fig. 2a has been widely used to represent the cross section

of blade. As seen from Fig. 2, the portions around leading and trailing edge of the airfoil are considered as nonstructural skin. The stiffness and mass of the nonstructural skin were ignored in the analysis. To control the design variables w and h, additional constraints were necessary to fit the rectangular box within the desired airfoil shape. To minimize the geometry errors in approximating a box beam airfoil, the present study suggests that all portions of the blade cross section be divided into a number of segments and spar caps. It is easy to generate the segments of desired airfoil using input data from the various airfoil coordinate information. Figure 2b shows the approximated airfoil model by 18 segments (for the skin and two spars) and 4 spar caps. The thicknesses of all segments are considered as design variables because they are the most important parameters on the blade weight and also on the blade aeroelastic behavior.

For numerical computation of the blade cross-sectional properties, each segment can be idealized by webs and two areas of effective longitudinals with effective distance between them, which guarantee equivalent area and area moment of inertial of the original shape as shown in Fig. 3a.[25] The effective longitudinals carry axial load only, and idealized webs carry shear stress only. In this study, the VR-7 airfoil is chosen, and the idealized structure is shown in Fig. 3b. The points in Fig. 3 are the effective longitudinals, and the numbers indicate the idealized webs. This approach allows systematic computations of not only the cross-sectional area, moment of inertia, bending stiffness, and torsional rigidity, but also the shear flows of each segment and the chordwise locations of center of gravity (c.g.), moment center (MC), and shear center (SC). Equations (1) and (2) show the calculations of these centers about y and z directions, respectively, and detailed procedures for shear flows and SC calculations are described in Refs. 25 and 26:

$$Y_{cg} = \frac{\sum_{i=1}^{n\text{long}} D_i A_i Y_i}{\sum_{i=1}^{n\text{long}} D_i A_i}, \qquad Y_{MC} = \frac{\sum_{i=1}^{n\text{long}} A_i^0 Y_i}{\sum_{i=1}^{n\text{long}} A_i^0}$$

$$Y_{SC} = 2\sum_{j=1}^{n\text{web}} A_j^{SC}(q_z)_j \tag{1}$$

$$Z_{cg} = \frac{\sum_{i=1}^{n\text{long}} D_i A_i Z_i}{\sum_{i=1}^{n\text{long}} D_i A_i}, \qquad Z_{MC} = \frac{\sum_{i=1}^{n\text{long}} A_i^0 Z_i}{\sum_{i=1}^{n\text{long}} A_i^0}$$

$$Z_{SC} = 2\sum_{j=1}^{n\text{web}} A_j^{SC}(q_y)_j \tag{2}$$

where $n$long and $n$web are the number of longitudinals and webs, respectively. These centers are considered as constraints to be placed at optimal locations. These sectional properties are dependent on the airfoil shape, the thicknesses, and the material properties of each segment.

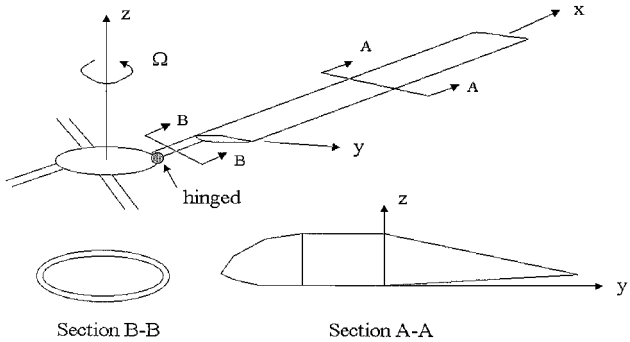

Fig. 1 Four-blade articulated rotor system and cross-section profiles.

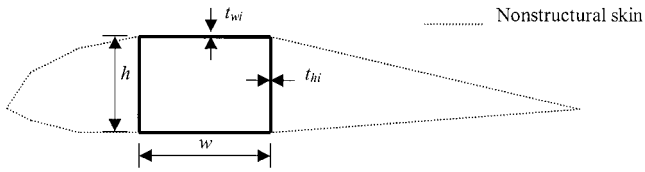

a) Simple box beam model

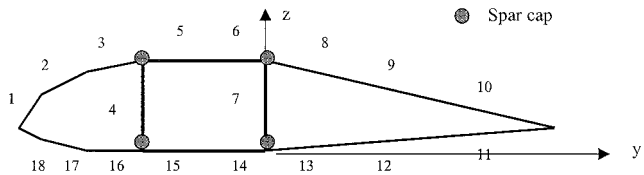

b) Complex model using finite segments and spar caps

Fig. 2 Comparison of rotor blade cross-section models.

Aerodynamic Force

The blade element theory, so-called strip theory, provides a model that allows one to determine the aerodynamic forces and moments acting on various spanwise elements. This approximate theory is based on an assumption that a rotor blade is composed of an assembly of aerodynamically independent airfoil elements and is appropriate for long, thin blades. This blade element theory can be combined with familiar momentum theory to determine flow conditions at each element.[19] These combined blade element and momentum theories can be an ideal application for the blade elastic analysis and are applied to calculate spanwise induced-velocity and aerodynamic lift coefficient distribution, which are the functions of rotor angular velocity, pitch angle, solidity ratio, and lift-curve slope. Unsteady airflow over chord and blade tip loss due to vortex formation are neglected in this paper.

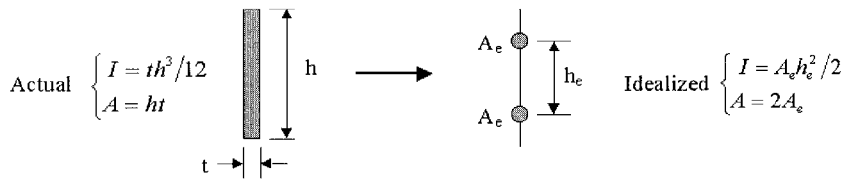

a) Idealization of each segment by two effective areas and webs

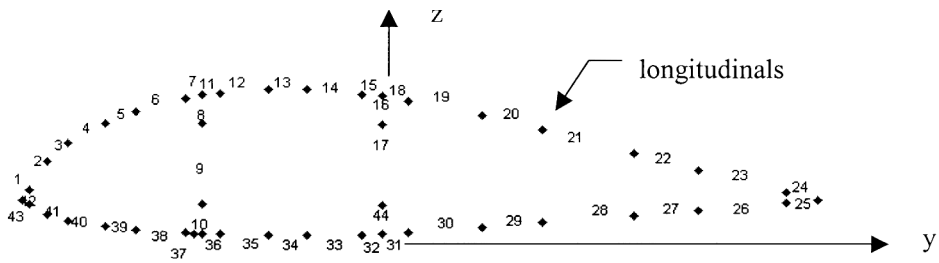

b) Idealized VR-7 airfoil using longitudinals and webs (numbers)

Fig. 3 Idealized structure.

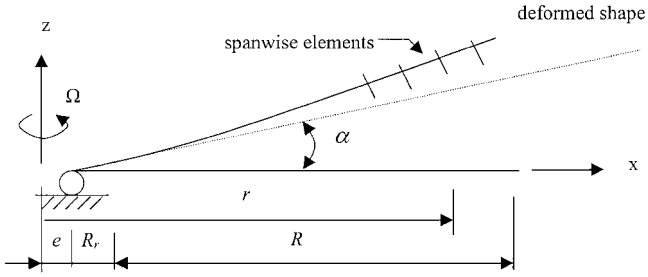

a) Boundary condition (hinged) and assumed deformed shape along the span

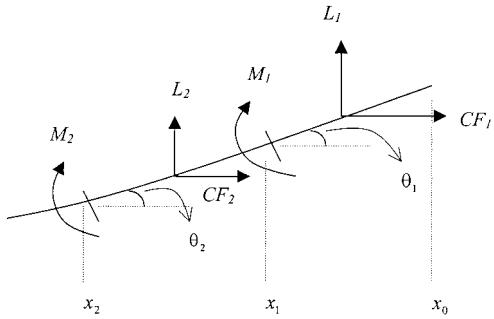

b) Elementary lift and centrifugal force distributions

Fig. 4 Discretizing blade as spanwise elements.

Discretizing Blade as Spanwise Elements

For conducting the blade elastic analysis with the aerodynamic force and moment, the blade is also divided into elements along the span direction. A rotating flexible blade with high tip speed undergoes large elastic deformations in axial, bending, and torsion. Figure 4a shows the boundary conditions of an articulated rotor blade, which is hinged at the hub, together with the assumed flapwise deformed shape along the span using second-order polynomial with respect to nondimensional spanwise coordinate as follows:

$$w = A[(r-e)/(R+R_r)]^2 + B[(r-e)/(R+R_r)] + C \qquad (3)$$

where w is the transverse deflection. The coefficient C equals zero because the displacement at the hinge is zero. The centrifugal forces (CFs) shown in Fig. 4b are expressed as follows:

$$\mathrm{CF}_k = \int_{x_k}^{x_{k-1}} \Omega^2 r m_k \, \mathrm{d}r \qquad (4)$$

where m_k is the mass of each element. The lift forces are

$$L_k = \int_{x_k}^{x_{k-1}} q_k c c_{lk} \, \mathrm{d}r \qquad (5)$$

where q_k is the dynamic pressure $1/2\rho_\infty (r\Omega)^2$ and c_{lk} is the elementary lift coefficients. The angles shown in Fig. 4b can be expressed as follows:

$$\theta_k = 2A[(r-e)/(R+R_r)] + B \qquad (6)$$

Therefore, the bending moment due to the lift and CFs at x_1 is

$$M_1 = L_1(d_1/2)\cos\theta_1 - \mathrm{CF}_1(d_1/2)\sin\theta_1 \qquad (7)$$

where d_1 is the length of the first element from blade tip. If θ_1 can be assumed to be small and all elements have the same length d, Eq. (7) can be linearized as

$$M_1 = L_1(d/2) - \mathrm{CF}_1(d/2)\theta_1 \qquad (8)$$

and the bending moment at x_2 can be

$$M_2 = L_2(d/2) - \mathrm{CF}_2(d_2/2)\theta_2 + L_1(d + d/2) - \mathrm{CF}_1(d\cdot\theta_2 + d/2\cdot\theta_1) \qquad (9)$$

The bending moment at the hinge, which can be expressed as the function of unknown coefficients A and B after continuing the earlier summation, should be zero for the hinged blade system. Because no more boundary conditions are given, the explicit solution for A and B cannot be obtained. If the value of B is given, the value of A can be determined, and the deformed shape can be obtained from Eq. (3). Therefore the value of B, which is identical to coning angle α in Fig. 4a, is taken as a variable and is increased from zero until it satisfies a static stability condition. When a value of α gives a maximum bending moment along the span that equals the absolute value of minimum bending moment shown as a thin continuous line in Fig. 5a, this α is called as α_{sta}, and this condition is considered the static stability condition in this research. If α is assumed to be smaller than α_{sta}, then the result will yield to overestimated bending moments due to CFs along the span (two dot lines in Fig. 5a). If α is assumed to be larger than α_{sta}, then the result will yield to overestimated bending moments due to lift forces along the span (two thick continuous lines in Fig. 5a). For each case, the flapwise deformed shapes from Eq. (3) are plotted in Fig. 5b. Of course, the α_{sta} is dependent on all of the design parameters such as the rotor angular velocity, pitch angle, blade radius, chord length, segment thicknesses, and so on.

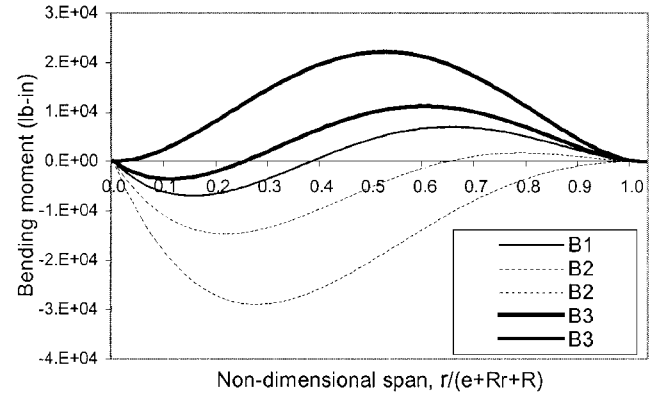

a) Bending moment distribution along the span as function of coning angle α

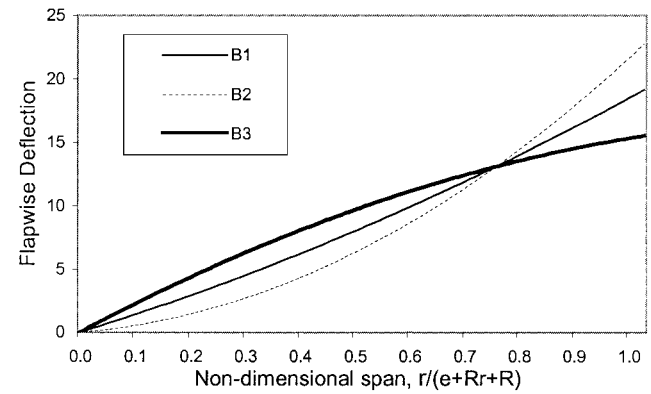

b) Flapwise deformed shape along the span as function of coning angle α (B1: $\alpha = \alpha_{\mathrm{sta}}$, B2: $\alpha < \alpha_{\mathrm{sta}}$, and B3: $\alpha > \alpha_{\mathrm{sta}}$)

Fig. 5 Coning angle to satisfy a static stability condition.

When the coefficients A and B are determined, the bending moments applied at each spanwise point ($x_1 \sim x_{\mathrm{nsp}}$) as well as the deformed shape can be calculated where nsp is the total number of spanwise elements and 113 elements are used to obtain precise results. The maximum twisting angle and maximum flapwise deflection are considered as constraints in the optimization process to be allowed less than reference values.

The discretization of the blade along the span makes evaluation of axial stresses due to centrifugal force and bending moment and shear stresses due to shear force and twisting moment possible. The total axial stress at each span station can be determined by using superposition of the stresses due to axial force and bending moment as follows:

$$(\sigma_{\mathrm{axial}})_{ki} = \mathrm{CF}_k/A_{\mathrm{cross}} + M_k(Z_i - Z_{\mathrm{MC}})\Big/ I_{yy}^{\mathrm{MC}} \qquad (10)$$

The total shear stress at each span station can be also determined by using superposition of the stresses due to shear force in the z direction (lift force) and twisting moment as follows:

$$(\sigma_{\text{shear}})_{kj} = (q_z)_{kj}\big/h_j^0 + (q_{Tl})_k\big/h_j^0 \tag{11}$$

The values of maximum axial and shear stress and their location on both chord and span direction can be obtained. In evaluating the maximum stress, the in-plane bending stress is negligible as compared with flapwise bending stress.

The design variables, the thicknesses of all segments, allow the material reassignment for chord direction only. Therefore, a thickness variation ratio (TVR) term is introduced in the design variables to allow linear variation of each segment thicknesses t_{is} along the span. TVR is defined as

$$\text{TVR} = (t_{\text{is}}|_{r=e+R_r})/t_{\text{is}M} \tag{12}$$

where subscript is indicates chordwise segment index and $t_{\text{is}M}$ is the segment thicknesses at the midspan. All segment thicknesses along the span direction are varied as a function of r:

$$t_{\text{is}}(r) = C_{\text{TVR}} \cdot t_{\text{is}M} \tag{13}$$

where

$$C_{\text{TVR}} = [(e + R_r + R/2) - r]/(R/2) \cdot (\text{TVR} - 1) + 1$$

The evaluation of cross-sectional properties is conducted once about midspan for numerical efficiency because the TVR does not affect the chordwise locations of c.g., MC, and SC along the span and also allows the linear variation on the other properties such as cross-sectional, area, moment of inertia, bending stiffness, and torsional rigidity. Therefore, the stress equations (10) and (11) are modified to include the effects of TVR as follows:

$$(\sigma_{\text{axial}})_{ki} = \frac{\text{CF}_k}{A_{\text{cross}}C_{\text{TVR}}} + \frac{M_k Z_i^*}{I_{yy}^{\text{MC}}C_{\text{TVR}}} \tag{14}$$

$$(\sigma_{\text{shear}})_{kj} = \frac{(q_z)_{kj}}{h_j^0 C_{\text{TVR}}} + \frac{(q_{Tl})_k}{h_j^0 C_{\text{TVR}}} \tag{15}$$

The limit margin of safety (MS) for shear and autorotational inertia (AI) are added in the constraints to ensure enough strength for shear stress and sufficient inertia:

$$\text{MS} = \frac{\text{yield stress}}{\text{applied limit stress}} - 1 \tag{16}$$

$$\text{AI} = \sum_{k=1}^{\text{nsp}} W_k \left(\frac{x_{k-1} + x_k}{2}\right)^2 \tag{17}$$

The margin of safety for tension (MS_{ten}) and total blade weight including blade root are taken as the objective function in the optimization process to be maximized and to be minimized, respectively. The reason of considering MS_{ten} as an objective function rather than a constraint is that it is difficult to constrain MS_{ten} as an explicit bound. The MS_{ten} is a critical parameter in a design for high tip speed lightweight blade, and the blade should have as high of a MS_{ten} as possible to prevent material failure or fatigue fracture. The total blade weight is

$$W_T = \rho_w(A_{\text{cross}}R + A_{\text{root}}R_r) + \text{tuning weight} \tag{18}$$

where ρ_w is the weight per unit volume and tuning weight will be introduced in the following rotor dynamic analysis.

Governing Equations for Dynamic Analysis

GATE

The blade dynamic analysis is performed for optimal natural frequency placement and vibratory vertical hub shear reduction.

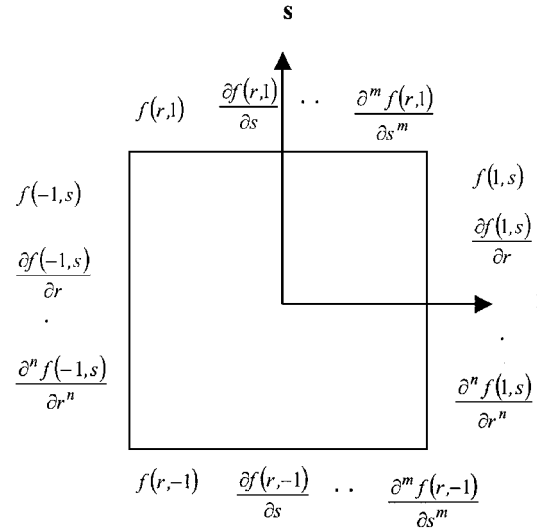

Fig. 6 GATE two-dimensional computational domains.

Hamilton's principle for a nonconservative elastic system is expressed as

$$\delta\int_{t1}^{t2}(T - V)\,\mathrm{d}t + \int_{t1}^{t2}\delta W\,\mathrm{d}t = 0 \tag{19}$$

where T, V, and W are the kinetic energy, strain energy, and external work, respectively. A high-order finite element (FE) from the GATE family is used to obtain more accurate results with less computational cost. The GATE family elements differ from the traditional FE in that they match not only a given function but also its derivatives up to a desired order exactly on every point along their boundaries. Figure 6 shows GATE family computational domain, and Eqs. (20–22) describe the GATE formulation using Boolean sum in two dimensions[22]:

$$P_r[f] = \sum_{i=-1}^{1}\left[f(i,s)b_{1/2(i+3)}(r) + \sum_{k=1}^{n}\frac{\partial^k f(i,s)}{\partial r^k}\frac{\partial^k b_{1/2(i+3)}(r)}{\partial r^k}\right] \qquad i \neq 0 \tag{20}$$

$$P_s[f] = \sum_{i=-1}^{1}\left[f(r,i)b_{1/2(i+7)}(s) + \sum_{k=1}^{m}\frac{\partial^k f(r,i)}{\partial s^k}\frac{\partial^k b_{1/2(i+7)}(s)}{\partial s^k}\right] \qquad i \neq 0 \tag{21}$$

$$f \cong \bar{f} \equiv (P_r \oplus P_s)[f] = P_r[f] + P_s[f] - P_rP_s[f] = \sum_{j=1}^{\text{ndof}} N_j f_j \tag{22}$$

where ndof indicates the number of degrees of freedom at each node, $b_{(i+j)}$ are blending functions, $f(i,s)$ and $f(r,i)$ are interpolation functions, and N_j are shape functions. Boolean sum yields the best approximation provided by the maximal projector, and $\bar{f}$ indicates an approximation to a given function f, which can be any variable such as geometry, field (displacement, rotation angle, and so on), and material. The system matrix from FE formulation based on Hamilton's principle yields

$$[M]\{\ddot{z}\} + ([K] + [K]_R)\{z\} = \{F\} \tag{23}$$

where $[M]$ is the global mass and $[K]$ and $[K]_R$ are the structural stiffness and centrifugal stiffening matrix due to rotating effect,[27] respectively. The damping effects are neglected and the aerodynamic force vector $\{F\}$ is equated to zero for free vibration analysis.

Equivalent Plate Model

In the elastic analysis, the arbitrary airfoil was modeled as a large number of segments, which allows the precise analyses of the cross-sectional properties and stress distributions. This model, however,

has some difficulties to be used in the FE analysis for the dynamic analysis because of the requirement of a great number of elements. Moreover, when the FE analysis is implemented into the optimization routine, it takes most of the computer time and space. Therefore, the equivalent plate thicknesses of an arbitrary airfoil, which are from the earlier idealized model of the blade cross section, can be separate input data for each mass and stiffness matrix of plate FE as follows:

$$t_{\text{mass}} = t_{\text{stiff\_in}} = A_{\text{cross}}/c, \qquad t_{\text{stiff\_ben}} = \left(12 \cdot I_{yy}^{\text{MC}}/c\right)^{\frac{1}{3}} \quad (24)$$

where t_{mass}, $t_{\text{stiff\_in}}$ and $t_{\text{stiff\_ben}}$ are equivalent plate thicknesses used in kinetic energy, strain energy for in-plane motion, and strain energy for flapwise bending, respectively. These thicknesses ensure that the cross section of the equivalent plate has the same area and area moment of inertia as the arbitrary airfoil without violating the aspect ratio of a rotor blade. The detailed procedures for application to these equivalent thicknesses are described in Ref. 26. This application can reduce the computational cost remarkably, and the accuracy was verified through the comparison with converged shell FE results obtained from commercial codes. The TVR effect is also taken into account in the FE analysis by multiplying C_{TVR} in Eq. (13) with the equivalent thicknesses given earlier along the span direction and then applying elementary average values to each FE.

Four-node eight GATE plate elements with nodal degrees of freedom u, v, v_x, w, w_x, w_y, and w_{xy} are used and resulted in converged values. The u, v, and w are the displacements with respect to the x, y, and z directions, and subscripts indicate the derivative with respect to x and y.

Vertical Hub Shear

The vertical shear contribution s_{ik} associated with response of the blade flapwise modes can be expressed in the form[20]

$$s_{ik} = q_{ik} \cdot \omega_i \int m\phi_i \, \mathrm{d}x \quad (25)$$

where q_{ik} indicates the response of ith mode subject to k per revolution, harmonic of airload, m is mass per unit length, and ω_i and ϕ_i are ith natural frequencies and eigenvectors, respectively. The amplitude of the s_{ik} can be expressed by the dynamic amplification factor DAF_{ik} and modal shaping parameter MSP_{ik} (Ref. 21):

$$S_{ik} = \text{MSP}_{ik} \cdot \text{DAF}_{ik} \cdot A_k \quad (26)$$

where

$$\text{MSP}_{ik} = \frac{\{U\}^T[M]\{\phi_i\} \cdot \{F_k\}\{\phi_i\}}{\bar{M}_i}$$

$$\text{DAF}_{ik} = \frac{(\omega_i/k\Omega)^2}{\sqrt{[(\omega_i/k\Omega)^2 - 1]^2 + (2\xi_i\omega_i/k\Omega)^2}}$$

A_k is the amplitude of aerodynamic force, and ξ_i is damping coefficient. The amplitudes of DAF are dependent on the blade natural frequencies and damping coefficient. The values of MSP can be controlled by the blade mode shapes ϕ_i, which can be tailored by tuning masses and their locations. The lumped tuning masses are positioned on the leading edge along the span direction. Their masses are taken into account in the FE analysis by dividing them and then applying them to adjacent FE nodes according to the proportion of the distance from each node using a linear interpolation function. The absolute value of the sum of vibratory hub shear forces of the first and second flapwise bending modes about per revolution is taken as the objective function in the optimization process to be minimized.[21]

Efficient Multilevel and Multiobjective Function Optimization

A general statement of optimization problem can be described mathematically with number of constraints (NCON) and number of design variables (NDV) as follows[28]:

$$\begin{aligned} &\text{minimize} && F(\bar{X}) && \text{(objective function)} \\ &\text{subject to} && g_i(\bar{X}) \le 0 && \text{(inequality constraints)} \quad i = 1, \text{NCON} \\ & && X_j^L \le X_j \le X_j^U && \text{(side constraints)} \quad j = 1, \text{NDV} \end{aligned} \quad (27)$$

where X are design variables. The superscripts L and U are the lower and the upper bounds, respectively. The side constraints are imposed to prevent the design variables from reaching unacceptable values.

The thicknesses of each segment, root wall thickness, TVR, and tuning masses and their positions are considered as design variables. For efficient analysis, the number of design variables for the segment thicknesses is reduced as follows:

$$\begin{gathered} t_a = t_1 = t_2 = t_3, \qquad t_b = t_4, \qquad t_c = t_5 = t_6, \qquad t_d = t_7 \\ t_e = t_8 = t_9 = t_{10}, \qquad t_f = t_{11} = t_{12} = t_{13} \\ t_g = t_{14} = t_{15}, \qquad t_h = t_{16} = t_{17} = t_{18} \end{gathered} \quad (28)$$

Three objective functions f_k taken in this study are the total weight to be minimized, f_1; the MS_{ten} to be maximized, f_2; and the vibratory hub shear to be minimized, f_3. The maximization is achieved simply by minimization of minus objective function. Scaling of objective function is required to avoid evaluating different objective functions in different units and to give a common basis for comparison[24]:

$$F_1 = c_1 f_1, \qquad F_2 = c_2 f_2, \qquad F_3 = c_3 f_3 \quad (29)$$

where F_1, F_2, and F_3 are scaled objective functions and c_1, c_2, and c_3 are the scaling factors determined at the starting design vector $\bar{X}^0$ as follows:

$$c_1 f_1(\bar{X}^0) = -c_2 f_2(\bar{X}^0) = c_3 f_3(\bar{X}^0) = \text{const} \quad (30)$$

For the multiobjective function optimization, the utility function formulation and global criterion formulation are applied.[24] In addition, a multilevel decomposition approach[29] is applied, and the results are compared with the other formulations.

Utility Function Formulation

A total utility function U to be minimized is defined as a linear combination of the objective functions[24]:

$$\begin{aligned} &\text{minimize} && U = w_1F_1 + w_2F_2 + w_3F_3 \\ &\text{subject to} && g_i(\bar{X}) \le 0 \qquad i = 1, \text{NCON} \end{aligned} \quad (31)$$

where w_1, w_2, and w_3 are the positive scalar weighting factors denoting relative importance of the objective functions. By the conversion of the multiobjective problem to a single objective one, the computational requirements are reduced as the same level as single objective optimization. However, it may be difficult to decide the weighting factors. In the test, all of the weighting factors are set as unit.

Global Criterion Formulation

In this formulation, the optimum design variable vector $\bar{X}$ is found by minimizing a global criterion $F(\bar{X})$ denoting the relative deviations of the individual objective functions from the optimal solutions[24]:

$$\begin{aligned} &\text{minimize} && F(\bar{X}) = \sum_{k=1}^{3} \left[\frac{F_k(\bar{X}) - F_k\left(\bar{X}_k^*\right)}{F_k\left(\bar{X}_k^*\right)} \right] \\ &\text{subject to} && g_i(\bar{X}) \le 0, \qquad i = 1, \text{NCON} \end{aligned} \quad (32)$$

where the design variable vectors $\bar{X}_k^*$ are obtained by optimizing the kth single objective function $F_k(\bar{X})$ subject to the same constraint set. This approach requires four outer iterations, three single and one global optimization, and the final design variable vector $\bar{X}$ can be obtained after the last iteration. A possible drawback of this technique is in more computational time requirement as compared to the utility function formulation.

Table 1 Constraint list

Constraint description	Upper or lower bound	Values used in the test
Blade natural frequency, per revolution		
First in plane	$f_1 \le f_1^U$	$f_1^U = 2.8$
First flapwise	$f_2^L \le f_2 \le f_2^U$	$f_2^L = 3.2,\ f_2^U = 3.8$
Second flapwise	$f_3^L \le f_3$	$f_3^L = 5.2$
MS for shear	$\mathrm{MS_{she}} \ge [\mathrm{MS_{she}}]_{\min}$	$[\mathrm{MS_{she}}]_{\min} = 1.0$
AI	$\mathrm{AI} \ge \mathrm{AI_{ref}}$	$\mathrm{AI_{ref}} = 0.8 \cdot \mathrm{AI_{initial\ value}}$
c.g. location	$[\mathrm{c.g.}/c]^L \le [\mathrm{c.g.}/c] \le [\mathrm{c.g.}/c]^U$	$[\mathrm{c.g.}/c]^L = 0.3,\ [\mathrm{c.g.}/c]^U = 0.45$
c.g./c from leading edge		
SC location	$[\mathrm{SC}/c]^L \le [\mathrm{SC}/c] \le [\mathrm{SC}/c]^U$	$[\mathrm{SC}/c]^L = 0.3,\ [\mathrm{SC}/c]^U = 0.4$
c.g./c from leading edge		
Maximum twisting angle, deg	$\phi_{\max} \le [\phi_{\max}]_{\mathrm{ref}}$	$[\phi_{\max}]_{\mathrm{ref}} = 3$
Maximum flapwise deflection, in. (mm)	$d_{\max} \le [d_{\max}]_{\mathrm{ref}}$	$[d_{\max}]_{\mathrm{ref}} = 30\ (762)$

Table 2 Fixed parameters

Fixed parameter	Value
Selected airfoil	VR-7
R_r, in. (mm)	33.0 (838.2)
R, in. (mm)	306.0 (7772)
$e/(e + R_r + R)$, %	3.0
c, in. (mm)	25.51 (648)
a, /rad	5.73
$c_{m,\mathrm{AC}}$	−0.01
AC/c, %	29.0
Ω, rad/s	25.66
Θ, deg	8.0
ρ_∞, slug/in.^{3} (kg/m^3)	1.38×10^{-6} (1.23)
Area of blade spar cap, in.^{2} (mm^2)	0.1 (645.1)
Speed of sound, ft/s (m/s)	1116.3 (340.3)
Material properties	
E, psi (N/m^2)	3.06×10^7 (21×10^{10})
ρ, lb/in.^{3} (kg/m^3)	0.298 (8.3×10^{10})
ν	0.3
Material yield strength, psi (N/m^2)	
Axial	5.50×10^4 (37.9×10^7)
Shear	2.75×10^4 (18.9×10^7)
Root shape (ellipsoid)	
Chord, in. (mm)	10.0 (254)
Height, in. (mm)	2.5 (63.5)

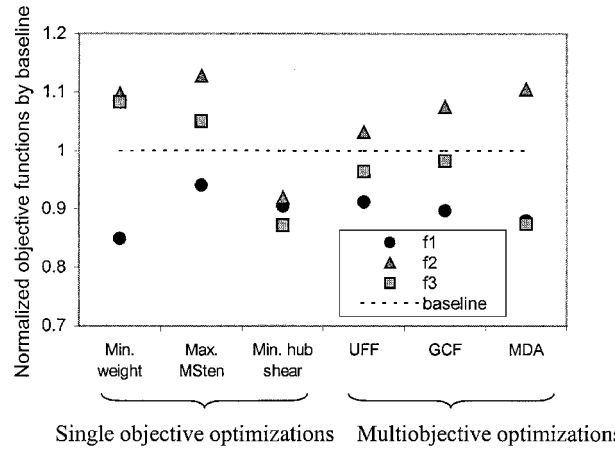

Fig. 7 Comparison of optimum solutions of normalized objective functions through single- and multiobjective function optimization techniques.

Multilevel Decomposition Approach

For efficient handling of the design variables and the objective functions together with their correlation, a multilevel decomposition approach is applied. In level 1 optimization, primary design for the minimum weight F_1 and maximum $\mathrm{MS_{ten}}$ F_2 are performed simultaneously using the global criterion formulation. The thicknesses of each segment, root wall thickness, and TVR, which affect these two objective functions directly, are considered as design variables in level 1 optimization. The usefulness of optimizing two objective functions using the global criterion formulation was verified in Refs. 30 and 31.

In level 2 optimization, secondary design for the minimum vibratory hub shear is performed by adding tuning masses. The magnitude of tuning masses and their positions, which affect this objective function directly, are considered as new design variables in level 2 optimization subjected to the same constraint set as level 1 optimization. Note that the final optimum values of the design variables on level 1 optimization are input values for level 2 optimization as fixed parameters, which means that they are no longer design variables. This approach also needs four outer iterations as the same level of computational requirements as optimizing three objective functions simultaneously using the global criterion formulation.

The program CONMIN[7] based on the method of feasible direction is used for the optimization, and the finite difference method is applied to calculate the first derivatives of the constraints and objective functions as an option in CONMIN.

Results and Discussion

Numerical results are obtained for four-blade rotor with aspect ratio 12 and 306 in. (7772.4 mm) of blade span length. Table 1 is a list of the constraints, and all constraints are applied as normalized form by the upper and lower bound. Table 2 is a list of the fixed parameters used in the test. Five different baseline sets (BS) are tested as described in Table 3. The only difference is the segment thicknesses. The tested problems consider only hovering flight with steady angular velocity. The calculated rotor thrust is 1.98×10^4 lb (8.81×10^4 N), tip Mach number is 0.67, and σ is 0.093.

Comparison of Multiobjective Optimization Techniques

The utility function formulation (UFF), global criterion formulation (GCF), and multilevel decomposition approach (MDA) are used for multiobjective optimization. The optimum solutions through these techniques using BS3 data are compared with single objective optimizations for each objective function. Figure 7 shows the normalized objective functions by the baseline values. The scaling factors c_1, c_2, and c_3 calculated from starting design variables are 2.79×10^{-3}, −1.306, and 0.541, respectively. The single objective optimizations yield good solutions for their corresponding objective functions only. The UFF and GCF yield the better solutions than the single objective optimizations. The MDA results in the best solutions among three multiobjective optimization techniques with respect to all of the objective functions.

Effects of Tuning Masses

An optimal location of the tuning mass is obtained through optimization procedure. Figure 8 shows the iteration history of the objective function in level 2 optimization of the MDA in a case of letting A_k in Eq. (26) be unit. The vibratory hub shear level is reduced remarkably after a few iterations except for BS1. The tuning mass is not applied in BS1 because the weight is not reduced through level 1 optimization. The upper limit of tuning mass is constrained by reduced weight through level 1 optimization as a side constraint. In all BSs except BS1, the optimal value of tuning mass increases slightly, and the position moves from 0.5 (/R) to 0.56 (/R).

Table 3 Design variables of BSs

Design variable	BS1	BS2	BS3	BS4	BS5
$t_a, t_b, t_c, t_d, t_e, t_f, t_g, t_h$, 10^{-2} in. (mm)	3.0 (76.2)	4.0 (101.6)	5.0 (127.0)	6.0 (152.4)	7.0 (177.8)
t_r, 10^{-1} in. (mm)	2.0 (50.8)	2.0 (50.8)	2.0 (50.8)	2.0 (50.8)	2.0 (50.8)
TVR	1.2	1.2	1.2	1.2	1.2
Tuning mass, lb (N)	15.0 (66.7)	15.0 (66.7)	15.0 (66.7)	15.0 (66.7)	15.0 (66.7)
TMP, /R	0.5	0.5	0.5	0.5	0.5

Table 4 Tests of three divided tuning masses and their locations in level 2 optimization

Test	Initial locations (/R)			Final locations (/R)			Hub shear, lb[a] (N) BS2	Hub shear, lb[a] (N) BS3
T-1	0.50	0.50	0.50	0.56	0.56	0.56	1.774 (7.891)	1.625 (7.228)
T-2	0.50	0.50	0.90	0.56	0.56	1.00	0.899 (3.999)	0.808 (3.594)
T-3	0.50	0.90	0.90	0.56	1.00	1.00	0.577 (2.566)	0.569 (2.531)
T-4	0.90	0.90	0.90	1.00	1.00	1.00	0.508 (2.260)	0.418 (1.859)

[a]Absolute values.

Table 5 Inspection of MSP and DAF[a] (BS2)

Test	MSP_{14}	DAF_{14}	S_{14}	MSP_{24}	DAF_{24}	S_{24}	S_4
No tuning Mass	−1.001	4.433	−4.439	0.647	1.322	0.856	−3.584
T-1	−0.994	2.682	−2.682	0.674	1.323	0.892	−1.774
T-4	−0.770	1.565	−1.206	0.477	1.462	0.698	−0.508

[a]In a case of $\xi = 0$.

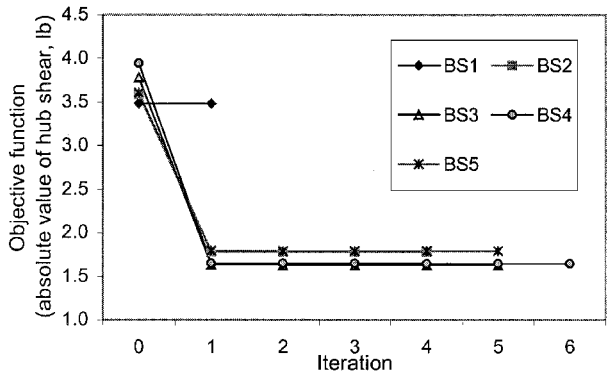

Fig. 8 Optimization iteration history of the objective functions in level 2 optimization of the MDA.

In level 2 optimization, more tests are conducted with different starting position of tuning mass to detect the local minimums. When the initial position is 0.9 (/R) instead of 0.5 (/R), the final position of tuning mass moves from 0.9 (/R) to 1.0 (/R). To investigate the effect of tuning mass in detail, the tuning mass is divided into three pieces, and then they are positioned on the different starting points. Table 4 shows the results, and the result of test 4 (T-4) yields an optimal solution on the view of the minimum hub shear with placing all tuning masses on the blade tip. Inspection of important parameters on the hub shear reduction shows that the amplitudes of DAF are more critical than MSP, as shown in Table 5. The first flapwise bending mode is the most critical one with frequency range from 3 to 4 per revolution. Figure 9 shows the changes of the mode shapes due to the tuning masses and their positions.

Existence of Local Minimums

The comparisons of optimum results of five different BSs in Table 3 through level 1 and 2 optimization of MDA are shown in Fig. 10. The increase of weight after level 2 optimization compared to level 1 optimization shown in Fig. 10a is due to the weight of the tuning masses. In the level 2 optimization, the initial positions of tuning masses are 0.9 (/R), then they move to 1.0 (/R) after

Table 6 Final optimums of the design variables of BS2 and BS3

BS	t_a	t_b	t_c	t_d	t_e	t_f	t_g	t_f	t_r	TVR	Tuning mass
BS2	3.41	3.81	3.93	4.92	2.68	2.79	4.12	3.91	1.99	1.2	18.84
BS3	5.02	5.31	5.50	5.86	2.70	2.81	5.42	5.10	2.01	1.2	21.24

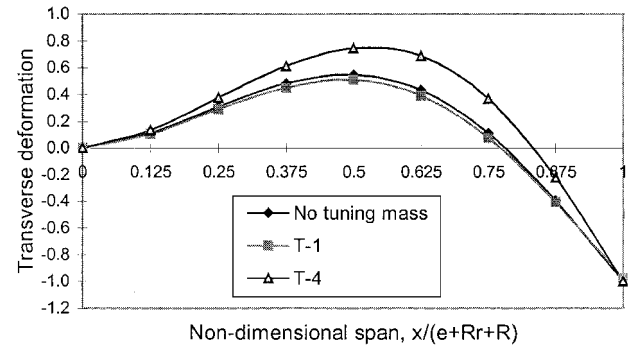

a) First flapwise mode

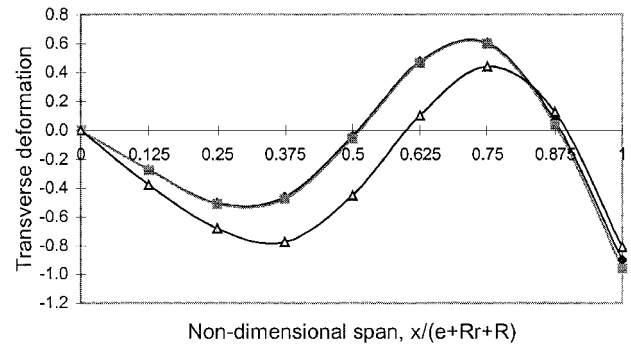

b) Second flapwise mode

Fig. 9 Comparison of mode shapes of three cases: no tuning mass and final results of T-1 and T-4 (BS2).

optimization for all BSs except BS1. The results of all BSs satisfy all required constraints except BS1. In BS1, the weight is not reduced, and the constraint MS_{she} is violated. In BS2, the most minimum weight can be achieved among the BSs along with a slightly higher vibratory hub shear than in BS3. In BS3, the smallest hub shear can be achieved among the BSs along with a slightly heavier weight than BS2. The BS4 and BS5 yield weighty blade and low MS_{ten} due to high centrifugal force even though they have high MS_{she}. Therefore, the BS2 and BS3 can be considered as the optimum input BSs. The well-defined initial values are important in optimization analysis. The final chordwise location of SC is 0.329 (/c) and c.g. is 0.428 (/c) from leading edge for BS2. In BS3, the final chordwise location of SC is 0.313 (/c) and c.g. is 0.402 (/c) from the leading edge. The natural frequencies of the first in-plane bending and first and second flapwise bending are successfully separated from the multiples of the driving frequencies 3, 4, and 5 prerevolution. For both BS2 and BS3, the maximum axial stress appears on the 17% span station from the blade root, and the maximum shear stress appears on the 15% span station and chordwise web number 17 (see Fig. 3b). The coning angle is 3.16 (deg) for BS2 and 2.60 for BS3, and tip deflection is 26.3 in. for BS2 and 21.5 for BS3.

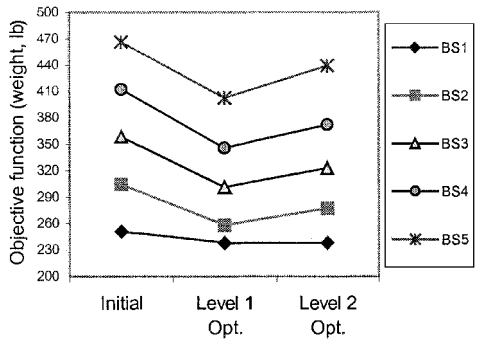

a) Minimize weight (objective function)

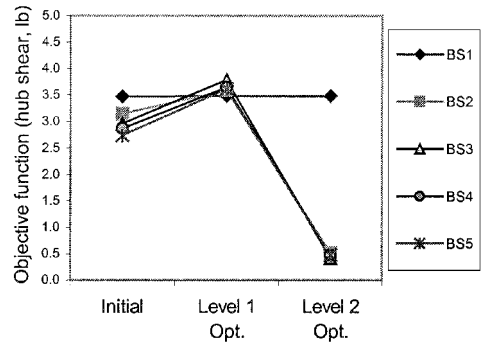

c) Minimize hub shear (objective function)

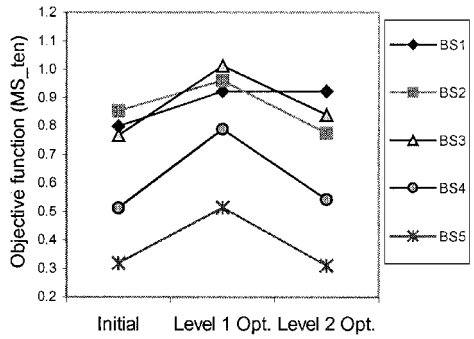

b) Maximize MS_{ten} (objective function)

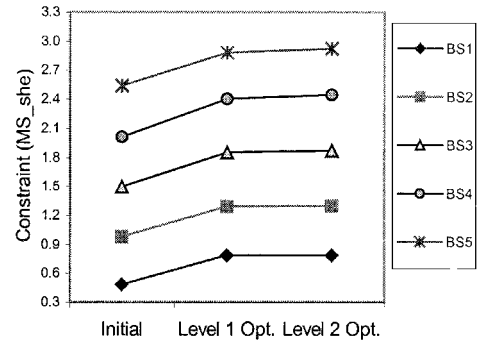

d) MS_{she} (constraint)

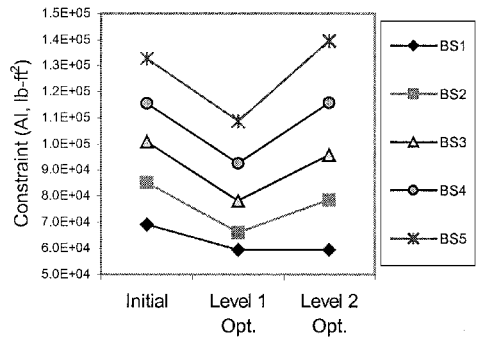

e) AI (constraint)

Fig. 10 Comparison of the initial and final results of the five BSs.

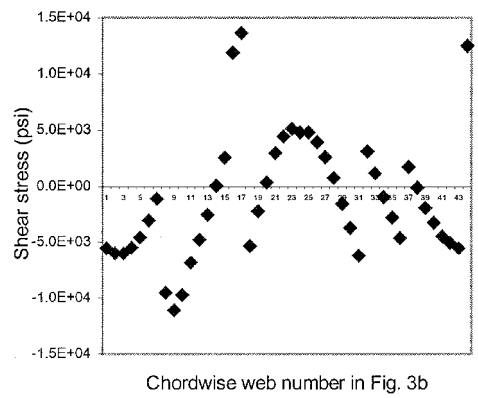

a) Initial result before optimization

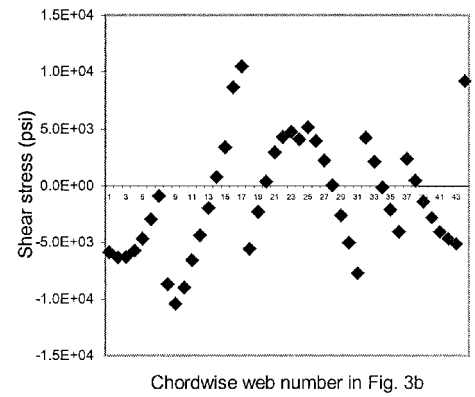

b) Final result after optimization

Fig. 11 Comparison of shear stress distribution on the blade cross section of midspan (BS2 result).

Figure 11 shows the comparison of initial and final shear stress distribution on the blade cross section of midspan based on the BS2 results. From the initial result, peak values of shear stress appear on the web numbers 16, 17, and 44, which are the idealized webs of segment number 7 shown in Fig. 2b. These peak values are reduced after optimization, as shown in Fig. 11b.

The final optimum values of the design variables of BS2 and BS3 are presented in Table 6. From final optimum values of the design variables, the spar thickness t_d is the thickest and carries the highest shear stress. The thicknesses of trailing edge t_e and t_f are the thinnest due to the constraints of SC and c.g. locations, which are placed as close to aerodynamic center as possible to minimize unwanted blade twisting.

Conclusions

An efficient multiobjective function optimization technique and its application to structural design of rotor blades with elastic and dynamic constraints have been described. The design study was a

high-aspect-ratioarticulated flexible blade with a thin-walled multicell cross section. During the optimization, to increase efficiency in numerical methods used in each discipline, a new analytical model using idealized structure and FE analysis from the GATE family was carried out for rotor elastic and dynamic analysis, respectively. The following conclusions are drawn based on the results of this presented study.

An analytical model discretizing the blade using both chordwise segments and spanwise elements provides the systematic computations about the chordwise locations of the c.g., MC and SC precisely, as well as the cross-sectional properties such as the area, moment of inertia, and torsional rigidity. This model also allowed the evaluations of axial stresses due to high centrifugal force and bending moment and shear stresses due to shear force and twisting moment. Through the optimization technique, this approach could guide the efficient material reassignment for both chordwise and spanwise directions to achieve minimum weight design.

An efficient FE using the equivalent plate model reduced the computational requirements and increased the accuracy for the rotor dynamic analysis.

For multiobjective function optimization, the UFF, GCF, and MDA were applied, and the results were compared with single-objective function optimizations. When multiobjective function optimization techniques were used, improved solutions could be found compared to single-objective function optimizations. Among the multiobjective optimization techniques, the MDA yielded the best solutions due to its efficient handling of the design variables and objective functions and their correlation.

In level 2 optimization of the MDA, the effects of tuning masses on vibratory vertical hub shear were investigated carefully with different starting points of the tuning masses. The results showed that the blade natural frequency placement is more important for hub shear reduction than the modal shaping. The first flapwise bending mode was the most critical one with frequency range from 3 to 4 per revolution on the tested problem. Remarkably minimum vibratory hub shear could be obtained by placing the tuning masses on the blade tip with a low mass penalty.

Many local optimums were found due to nonlinearities of both the constraints and the objective functions. The existence of local minimums is one of the weak points of any gradient-based optimization algorithm, and the use of different starting values may be necessary to achieve good results.

References

[1]Miura, H., "Applications of Numerical Optimization Mehods to Helicopter Design Problems—A Survey," *Vertica*, Vol. 9, No. 2, 1985, pp. 141–154.

[2]Friedmann, P. P., "Helicopter Rotor Dynamics and Aeroelasticity: Some Key Ideas and Insights," *Vertica*, Vol. 14, No. 1, 1990, pp. 101–121.

[3]Friedmann, P. P., "Helicopter Vibration Reduction Using Structural Optimization with Aeroelastic/Multidisciplinary Constraints—A Survey," *Journal of Aircraft*, Vol. 28, No. 1, 1991, pp. 8–21.

[4]Celi, R., "Recent Applications of Design Optimization to Rotorcraft—A Survey," *Journal of Aircraft*, Vol. 36, No. 1, 1999, pp. 176–189.

[5]Peters, D. A., Ko, T., Korn, A., and Rossow, M. P., "Design of Helicopter Rotor Blades for Desired Placement of Natural Frequencies," *Proceedings of the 39th Annual National Forum of the American Helicopter Society*, American Helicopter Society, Washington, DC, 1983, pp. 674–689.

[6]Peters, D. A., Rossow, M. P., Korn, A., and Ko, T., "Design of Helicopter Rotor Blades for Optimum Dynamic Characteristics," *Computers and Mathematics with Applications*, Vol. 12A, No. 1, 1986, pp. 85–109.

[7]Vanderplaats, G. N., "CONMIN—A Fortran Program for Constrained Function Minimization," User's Manual, NASA TM X-62282, Aug. 1973.

[8]Friedmann, P., "Application of Modern Structural Optimization to Vibration Reduction in Rotorcraft," *Vertica*, Vol. 9, No. 4, 1985, pp. 363–376.

[9]Walsh, J. L., Bingham, G. J., and Riley, M. F., "Optimization Methods Applied to the Aerodynamic Design of Helicopter Rotor Blades," *Journal of the American Helicopter Society*, Vol. 32, No. 4, 1987, pp. 39–44.

[10]Chattopadhyay, A., and Walsh, J. L., "Minimum Weight Design of Helicopter Rotor Blades with Frequency Constraints," *Journal of the American Helicopter Society*, Vol. 34, No. 4, 1989, pp. 77–82.

[11]Chattopadhyay, A., Walsh, J. L., and Riley, M. F., "Integrated Aerodynamic Load/Dynamic Optimization of Helicopter Rotor Blades," *Journal of Aircraft*, Vol. 28, No. 1, 1991, pp. 58–65.

[12]Weller, W. H., and Davis, M. W., "Wind Tunnel Tests of Helicopter Blade Design Optimized for Minimum Vibration," *Journal of the American Helicopter Society*, Vol. 34, No. 3, 1989, pp. 40–50.

[13]Celi, R., and Friedmann, P. P., "Structural Optimization with Aeroelastic Constraints of Rotor Blades with Straight and Swept Tips," *AIAA Journal*, Vol. 28, No. 5, 1990, pp. 928–936.

[14]Lim, J. W., and Chopra, I., "Aeroelastic Optimization of a Helicopter Rotor Using an Efficient Sensitivity Analysis," *Journal of Aircraft*, Vol. 28, No. 1, 1991, pp. 29–37.

[15]Adelman, H. M., and Mantay, W. R., "Integrated Multidisciplinary Design Optimization of Rotorcraft," *Journal of Aircraft*, Vol. 28, No. 1, 1991, pp. 22–28.

[16]He, C. J., and Peters, D. A., "Optimization of Rotor Blades for Combined Structural, Dynamic, and Aerodynamic Properties," *Structural Optimization*, Vol. 5, No. 1–2, 1992, pp. 37–44.

[17]Ganguli, R., and Chopra, I., "Aeroelastic Optimization of a Helicopter Rotor with Two-Cell Composite Blades," *AIAA Journal*, Vol. 34, No. 4, 1996, pp. 835–841.

[18]Yuan, K. A., and Friedmann, P. P., "Structural Optimization for Vibratory Loads Reduction of Composite Helicopter Rotor Blades with Advanced Geometry Tips," *Journal of the American Helicopter Society*, Vol. 43, No. 3, 1998, pp. 246–256.

[19]Stepniewski, W. Z., *Rotary-Wing Aerodynamics*, Dover, New York, 1978, pp. 91–100.

[20]Taylor, R. B., "Helicopter Vibration Reduction by Rotor Blade Modal Shaping," *Proceedings of the 38th Annual Forum of the American Helicopter Society*, American Helicopter Society, Washington, DC, 1982, pp. 90–101.

[21]Pritchard, J. I., and Adelman, H. M., "Optimal Placement of Tuning Masses for Vibration Reduction in Helicopter Rotor Blades," *AIAA Journal*, Vol. 28, No. 2, 1990, pp. 309–315.

[22]Sarigul-Klijn, N., "On the Formulation of Gradient Adaptive Transfinite Elements," *Steep Gradients and Finite Element Method*, NSK, Davis, CA, 1997.

[23]Sarigul-Klijn, N., "A Modal Synthesis Approach for Dynamic Response of Space Vehicle Systems," American Society of Mechanical Engineers, ASME Paper DAS-RH-P14, Nov. 1998.

[24]Rao, S. S., "Multiobjective Optimization in Structural Design with Uncertain Parameters and Stochastic Processes," *AIAA Journal*, Vol. 22, No. 11, 1984, pp. 1670–1678.

[25]Rivello, R. M., *Theory and Analysis of Flight Structures*, McGraw–Hill, New York, 1969, pp. 133–223.

[26]Kim, J. E., "An Approach to Elastic–Dynamic–Aeroelastic Multiobjective Optimization of Rotor Blades," Ph.D. Dissertation, Mechanical and Aeronautical Engineering Dept., Univ. of California, Davis, CA, June 2000.

[27]Bhat, R. B., "Transverse Vibrations of a Rotating Uniform Cantilever Beam with Tip Mass as Predicted by Using Beam Characteristic Orthogonal Polynomials in the Rayleigh–Ritz Method," *Journal of Sound and Vibration*, Vol. 105, No. 2, 1986, pp. 199–210.

[28]Vanderplaats, G. N., *Numerical Optimization Techniques for Engineering Design with Application*, McGraw–Hill, New York, 1984, pp. 313–325.

[29]Chattopadhyay, A., McCarthy, T. R., and Pagaldipti, N., "A Multilevel Decomposition Procedure for Efficient Design Optimization of Helicopter Rotor Blades," *Proceedings of the ARO–AHS 5th International Workshop on Dynamics and Aeroelastic Stability*, NASA Langley Research Center, Hampton, VA, 1993, pp. 183–195.

[30]Kim, J. E., and Sarigul-Klijn, N., "An Application of Multidisciplinary Optimization to an Articulated Rotor Blade in High Speed," *Proceedings of Opti_CON'99*, Long Beach, CA, 1999, pp. 27–35.

[31]Kim, J. E., and Sarigul-Klijn, N., "Structural Optimization for Lightweight Articulated Rotor Blade," AIAA Paper 2000-1520, April 2000.

A. Chattopadhyay
Associate Editor